SSRG International Journal of Mechanical Engineering
ISSN: 2348-8360/ https://doi.org/10.14445/23488360/IJME-V13I1P101

Volume 13 Issue 1, 1-13, January 2026

Original Article

A Closed-Form Analytical Solution for Crack Interaction in Orthotropic Plates with Multiple Holes under Combined Load

Lakshminarayana N P[1], Chandra Mohan Reddy B[2]

[1,2]*Department of Mechanical Engineering, JNTUA Anantapur, Andhra Pradesh, India.*

[1]*Corresponding Author : laxmi512@gmail.com*

Received: 02 November 2025 Revised: 03 December 2025 Accepted: 02 January 2026 Published: 14 January 2026

Abstract *- This work presents an analytical solution for the radial cracks emanating from three circular holes in an infinite orthotropic plate under in-plane combined biaxial and shear loading. A closed-form solution that takes into account the interaction effects between cracks is obtained by combining Schwarz's alternating method with the complex variable approach. MATLAB is used to assess the normalized Stress Intensity Factors (SIFs) at the crack tips under combined loading conditions. The impact of important factors on the normalized SIFs is methodically examined, including fiber orientation, crack angle, material orthotropy, crack length, and center-to-center hole spacing. The findings show that longer cracks have higher SIF ratios, with the inner crack tip experiencing greater intensity than the outer one, while an increase in hole spacing results in a decrease in the normalized SIF ratio, which approaches unity. The analytical results demonstrate good agreement with deviations of less than 6% when compared to ANSYS finite element simulations. The suggested analytical framework can be successfully applied to real-world fracture mechanics issues involving composite and orthotropic materials and offers a dependable and effective method for evaluating crack interaction effects in orthotropic plates.*

Keyword *- Analytical method, Crack angle, Crack interaction, Orthotropic plate, Stress Intensity Factor (SIF).*

1. Introduction

In many critical engineering structures, such as aircraft bodies, rocket casings, ship hulls, and pressure vessels, holes are intentionally created to accommodate fasteners and joints. During service, these holes are subjected to complex loading, which gives rise to high stress concentrations in the surrounding material, particularly in orthotropic composite systems. Under such operating conditions, cracks tend to initiate at the edges of the holes beneath fastener heads and then propagate along paths influenced by both the applied loads and the directional properties of the material. In modern lightweight structural designs, where safety margins are intentionally reduced to satisfy weight and cost requirements, even limited crack growth can quickly endanger structural integrity. For this reason, dependable fracture assessment methods that can realistically account for crack interaction effects are essential for structural designers and integrity engineers.

Although existing fracture mechanics models offer useful insight for isolated holes or single-crack cases, real engineering structures often contain multiple fastener holes located close to one another. In these situations, the stress fields associated with neighboring holes and cracks interact, resulting in stress intensity factors that can differ significantly from those predicted using single-hole assumptions. This Effect is especially notable in orthotropic composite materials, where directional stiffness further alters the stress distribution. As a consequence, simplified models that ignore interaction effects may lead to inaccurate life predictions and potentially unsafe designs. Despite its clear practical relevance, the problem of interacting cracks in multi-hole configurations has received limited analytical attention.

As the use of composite and anisotropic materials in engineering applications increased, research focus gradually shifted toward the analysis of orthotropic and laminated plates. Moussavian and Jafari [1] and Hajimohamadi and Ghajar [2], who examined the impact of material anisotropy on Stress Intensity Factors (SIFs), reported analytical solutions for cracks originating from a single circular hole in orthotropic or quasi-orthotropic plates. Catalanotti and Salgado [3] further analysed the crack originating from a single hole in orthotropic plates, emphasizing the function of directional stiffness. While Goleij et al. [5] used continuously distributed dislocation arrays to assess SIFs at crack tips, Beam and Cui [4] used the complex variable method in conjunction with linear transformation techniques to derive

SIFs for cracks originating from a circular hole in orthotropic materials. Kushch and Sevostianov [6] and Huang et al. [7] proposed alternative analytical methods, including orthotropy rescaling and elliptical hole modelling, extending the applicability of these solutions to more general geometries and loading conditions.

Ukadgaonker and Sharma [8] advanced the study and gave SIF solutions for cracks subjected to internal pressure in laminated composite plates, by accounting for the coupling effects between layers. While Zhao [9] proposed an analytical method for evaluating SIFs in infinite plates containing multiple hole-edge cracks, the application was largely restricted to isotropic materials. Yan [10] gave SIF expressions for cracks emanating from circular holes in finite rectangular plates under tensile loading, while Liu and Duan [11] provided analytical solutions for cracks emanating from elliptic holes in infinite plates.

Beyond analytical methods, numerical and experimental paradigms have been widely used to study crack behaviour in plates with openings. Harilal et al. [12] utilized digital image correlation to calculate SIFs for various crack configurations, offering valuable experimental validation. Kim and Paulino [13] applied the numerical displacement correlation technique to assess SIFs in orthotropic plates.

Cheong and Hong [14] studied mixed-mode crack behaviour emanating from circular holes in orthotropic materials, highlighting the Effect of material anisotropy on mode coupling. Fu and Zhang [15] also presented an analytical–variational approach to determine SIFs for cracks emanating from holes in both isotropic and anisotropic plates, offering a link between purely analytical solutions and numerical methods. Studies reported in [16-25] provided stress distributions around multiple holes in isotropic and orthotropic plates under different loading conditions.

Despite significant advances in the study of cracks originating from single holes and, to some extent, from multiple holes, strong analytical solutions that completely capture interaction effects among multiple cracked holes in orthotropic plates are still lacking. A review of available studies shows that no closed-form solution has yet been presented for an orthotropic plate with three circular holes, each containing two cracks, subjected to combined biaxial and shear loading while accounting for interaction effects. This unresolved problem restricts the applicability of present models to practical engineering applications.

For the structure shown in Figure 1, this work provides a closed-form analytical solution for an orthotropic plate with three circular holes, each of which has two cracks, subjected to combined biaxial and shear loads at infinity. The formulation uses Schwarz's alternating method in conjunction with the Kolosov–Muskhelishvili complex variable approach to accurately capture multi-hole interaction effects and to evaluate stress intensity factors directly, without the need for repeated finite-element re-meshing. The Effect of hole spacing, crack length and orientation, fiber angle, and material orthotropy on normalized mode-I and mode-II stress intensity factors is highlighted by a parametric analysis. The findings show that crack orientation and fiber angle are critical factors in fracture severity; closely spaced holes greatly enhance interaction effects, especially at inner crack tips.

By addressing the limitations of previous studies, this work proposes a novel analytical closed-form solution of a three-hole, multi-crack problem in an orthotropic plate, and by considering the interaction effects under combined loading. These contributions greatly advance our knowledge of fracture behavior in fastener-dense orthotropic composite structures and offer a useful analytical framework for damage-tolerant design.

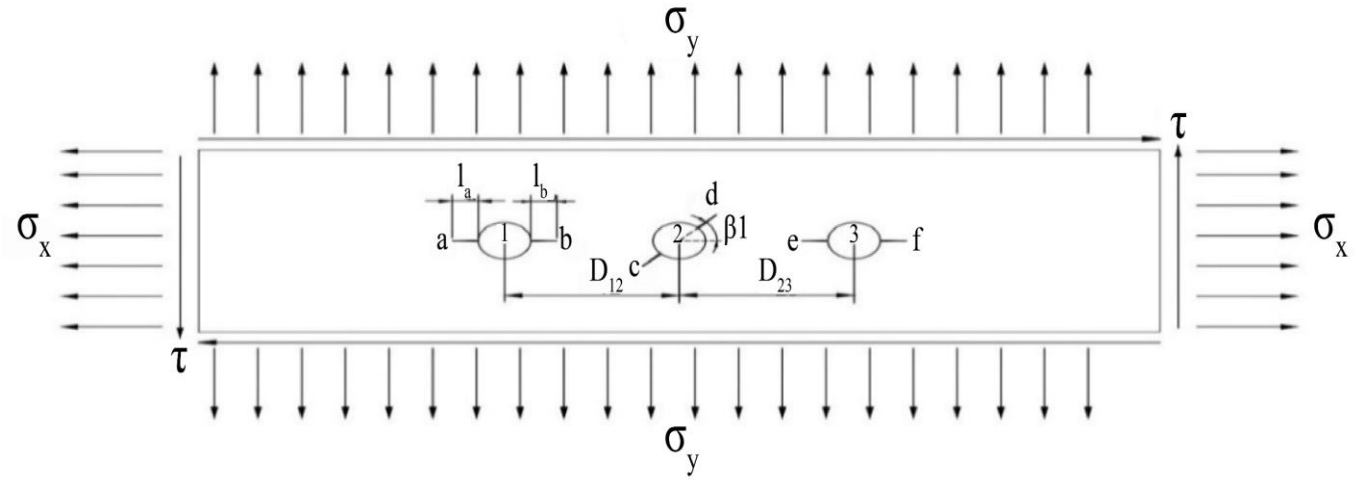

Fig. 1 Infinite orthotropic plate with three holes and a cracks system subjected to Bi-Axial+Shear loading at infinity

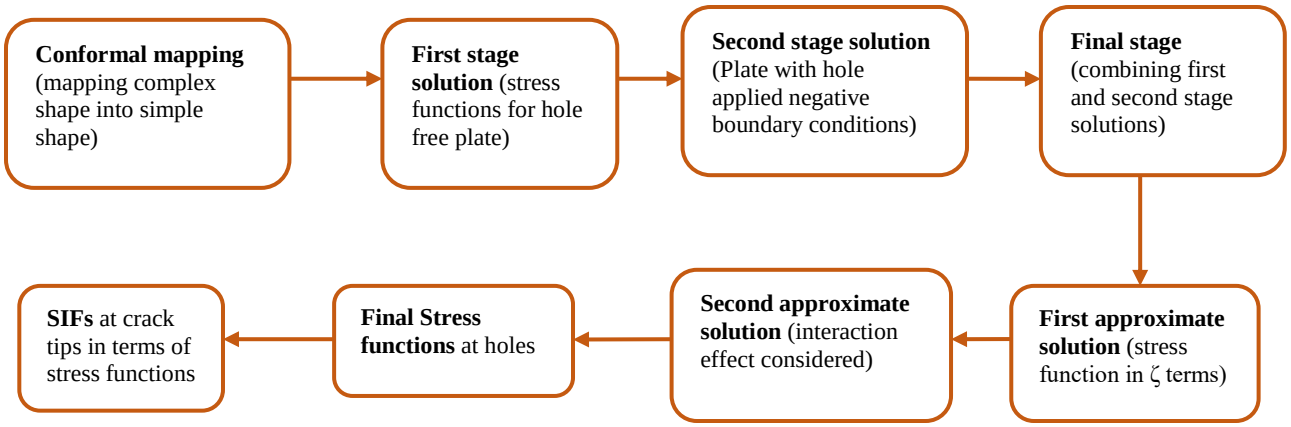

Fig. 2 Steps in determining SIFs at crack tips by complex variable method

2. Methodology

The aim of the present work is to obtain the complex stress functions, Stress Intensity Factors (SIFs), and to analyze the interaction effects in an orthotropic plate featuring three holes, each with two arbitrarily oriented radial cracks, under combined biaxial and shear loading at infinity. The following analytical methods can be employed to calculate SIF in an orthotropic plate.

1. Complex Variable Method (CVM)
2. The method of dislocation arrays
3. CVM combined with integral equations
4. Orthotropy rescaling method

In this paper, the CVM is utilized to obtain an analytical solution to the aforementioned problem. This method allows for the straightforward resolution of complex geometries with arbitrary loading through the principles of complex variables. The steps involved in determining the SIFs at the crack tip are illustrated in Figure 2. The procedure for obtaining a solution for a plate with three holes, each with two cracks, under combined loading is divided into several stages. These stages include mapping the complex shape to a simple shape through a mapping procedure [1, 14], developing stress functions for the combined loading, and providing solutions in stages: the first stage solution, the second stage solution, and the final stage solution [8]. This process also involves determining the first and second approximate solutions, followed by calculating the SIF equations at the crack tips.

The following assumptions are made in the derivation:
1. Material is linearly

2.1. Complex Variable Formulation for Combined Loading

The CVM is employed to derive the analytical solution for the current problem, with the loading conditions specified as follows.

$$\sigma_x = \lambda P;\ \sigma_y = P;\ \tau_{xy} = P; \text{ at infinity} \quad (1)$$

Taking into account the generalized plane stress condition for a thin orthotropic plate, Airy's stress functions are introduced and substituted into the compatibility equation to derive the characteristic equation for in-plane loading [1].

$$a_{1_1}s^4 - 2a_{1_6}s^3 + (2a_{1_2} + a_{6_6})s^2 - 2a_{2_6}s + a_{2_2} = 0 \quad (2)$$

The roots of the above bi-harmonic equation are,

$$s_1 = \alpha_1 + i\gamma_1$$

$$s_2 = \alpha_2 + i\gamma_2$$

$$s_3 = \alpha_1 - i\gamma_1$$

$$s_4 = \alpha_2 - i\gamma_2$$

2.2. Mapping Procedure

The initial phase of mathematical formulation involves mapping, utilizing the conformal mapping technique to transform complex shapes, such as a circular hole with a cracked opening in the z-plane, into a known simple shape, like the unit circle in the ζ-plane, through the application of the conformal mapping function [1, 8, 14].

$$z_j = w_j(\zeta) = (M) * \left[(a_j + b_j)\left(\frac{1}{\zeta} + \zeta\right)\right] + N \quad (3)$$

Where, for a circular hole $a_j = 1 + is_j\ b_j = 1 - is_j$, j=1,2. Hole size constants [1] given as,

$$M = \frac{1}{8}\left(2 + l_r + l_l + \frac{1}{1 + l_r} + \frac{1}{1 + l_l}\right)$$

$$N = \frac{1}{4}\left((l_r - l_l) + \frac{1}{1 + l_r} - \frac{1}{1 + l_l}\right)$$

Where l_r and l_l represent the lengths of the right and left crack, respectively.

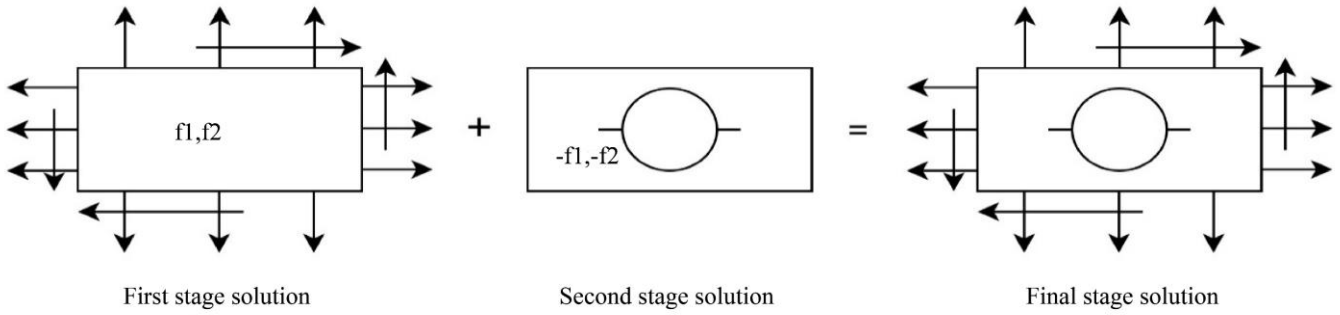

Fig. 3 Stages in determining stress functions at the hole

2.3. Determining Stress Functions for Holes

After transforming the complex shape into a unit circle, stress functions for the combined loading case [8] were derived in the stages shown in Figure 3.

2.3.1. First Stage

In the first stage, the stress functions $\phi_1(z_1)$, $\varphi_1(z_2)$ [23] are derived for a hole-free plate subjected to remote in-plane loading at infinity.

$$\phi_1(z_1) = B_1 z_1 \tag{4}$$

$$\varphi_1(z_2) = (B_2 + iC_2)\, z_2 \tag{5}$$

Where,

$$B_1 = \frac{\sigma_x+(\alpha_2^2+\gamma_2^2)\sigma_y+2\alpha_2\tau_{xy}}{2[(\alpha_2-\alpha_1)^2+(\gamma_2^2-\gamma_1^2)]} \tag{6}$$

$$B_2 = \frac{-\sigma_x+(\alpha_1^2-\gamma_1^2-2\gamma_1\gamma_2)\sigma_y-2\alpha_2\tau_{xy}}{2[(\alpha_2-\alpha_1)^2+(\gamma_2^2-\gamma_1^2)]} \tag{7}$$

$$C_2 = \frac{\sigma_x(\alpha_1-\alpha_2)+\left(\alpha_2(\alpha_1^2-\gamma_1^2)-\alpha_1(\alpha_2^2-\gamma_2^2)\right)\sigma_y+\left((\alpha_1^2-\gamma_1^2)-(\alpha_2^2-\gamma_2^2)\right)\tau_{xy}}{2\gamma_2[(\alpha_2-\alpha_1)^2+(\gamma_2^2-\gamma_1^2)]} \tag{8}$$

The boundary conditions [1] f_1 and $f_2$for the imaginary hole are subsequently derived from the stress functions.

$$f_1 = 2Re\left[(G_1+G_2)\left(\zeta+\frac{1}{\zeta}\right)+N\right] \tag{9}$$

$$f_2 = 2Re\left[(G_3+G_4)\left(\zeta+\frac{1}{\zeta}\right)+N\right] \tag{10}$$

Where,

$$G_1 = M[B_1a_1 + (B_2+iC_2)a_2] \tag{11}$$

$$G_2 = M[B_1b_1 + (B_2+iC_2)b_2] \tag{12}$$

$$G_3 = M[s_1B_1a_1 + s_2(B_2+iC_2)a_2]s \tag{13}$$

$$G_4 = M[s_1B_1b_1 + s_2(B_2+iC_2)b_2] \tag{14}$$

2.3.2. Second Stage

At the second stage, the solution considers a plate with a hole, on which boundary conditions equal in magnitude and opposite sign (f_1^0= - f_1 and f_2^0= - f_2) are imposed on its hole boundary, without any remote loading. The stress functions of the second stage solution $\phi_0(z_1)$, $\varphi_0(z_2)$ are derived from these boundary conditions by substituting into the Schwarz formula [17]. After evaluating the Schwarz formula and evaluating the integral, the stress functions are obtained as [1, 23]

$$\phi_0(\zeta) = \frac{1}{s_1-s_2}\left\{\left(\frac{1}{\zeta}\left(s_2\left(G_1+\overline{G_2}\right)-\left(G_3+\overline{G_4}\right)\right)+\frac{1}{\zeta^2}\left(s_2\left(G_2+\overline{G_1}\right)-\left(G_4+\overline{G_3}\right)\right)+N\right)\right\} \tag{15}$$

$$\varphi_0(\zeta) = \frac{-1}{s_1-s_2}\left\{\left(\frac{1}{\zeta}\left(s_1\left(G_1+\overline{G_2}\right)-\left(G_3+\overline{G_4}\right)\right)+\frac{1}{\zeta^2}\left(s_1\left(G_2+\overline{G_1}\right)-\left(G_4+\overline{G_3}\right)\right)+N\right)\right\} \tag{16}$$

2.3.3. Final Stage

In the final stage, the final stress functions $\phi(z_1)$,$\varphi(z_2)$ for a hole are obtained through superposition of the solution from the first and second stages [1, 23].

$$\phi(z_1) = \phi_1(z_1) + \phi_0(z_1) \tag{17}$$

$$\varphi(z_2) = \varphi_1(z_2) + \varphi_0(z_2) \tag{18}$$

2.3.4. First Approximate Solution

In the first approximate solution, stress functions for all three holes are expressed as a function of ζ. The stress functions corresponding to the first, second, and third holes are denoted as $\phi_1(\zeta_1)$, $\varphi_1(\zeta_1)$; $\phi_2(\zeta_2)$, $\varphi_2(\zeta_2)$; $\phi_3(\zeta_3)$, $\varphi_3(\zeta_3)$; these functions do not account for interaction effects from neighboring holes. For a plate with three holes and two radial cracks emanating from each hole, the hole size constants for the first, second, and third holes are represented by M_1, M_2, and M_3, respectively. $M_1 = \frac{1}{8}\left(2+l_a+l_b+\frac{1}{1+l_a}+\frac{1}{1+l_b}\right)$ $M_2 = \frac{1}{8}\left(2+l_c+l_d+\frac{1}{1+l_c}+\frac{1}{1+l_d}\right)$ $M_3 = \frac{1}{8}\left(2+l_e+l_f+\frac{1}{1+l_e}+\frac{1}{1+l_f}\right)$

Where R_1, R_2, and R_3 represent the radii of the holes, and l_a or a, l_b or b, $l_c$or c, l_d or d, l_e or e, and l_f or f denote the crack

lengths at 1st,2nd, and 3rd holes respectively, β_1 indicates the crack angle at the second hole. The stress functions for the first hole,

$$\phi_1(\zeta_1) = \frac{1}{s_1-s_2}\left\{\frac{1}{\zeta_1}\left(s_2\left(G_1+\overline{G_2}\right)-\left(G_3+\overline{G_4}\right)\right)+\frac{1}{{\zeta_1}^2}\left(s_2\left(G_2+\overline{G_1}\right)-\left(G_4+\overline{G_3}\right)\right)+N_1\right\}+B_1 z_{11} \quad (19)$$

$$\varphi_1(\zeta_1) = \frac{-1}{s_1-s_2}\left\{\frac{1}{\zeta_1}\left(s_1\left(G_1+\overline{G_2}\right)-\left(G_3+\overline{G_4}\right)\right)+\frac{1}{{\zeta_1}^2}\left(s_1\left(G_2+\overline{G_1}\right)-\left(G_4+\overline{G_3}\right)\right)+N_1\right\}+(B_2+iC_2)z_{21} \quad (20)$$

Where,

$$z_{11} = M_1(a_1+b_1)\left(\zeta_1+\frac{1}{\zeta_1}\right)+N_1 \quad (21)$$

$$z_{21} = M_1(a_2+b_2)\left(\zeta_1+\frac{1}{\zeta_1}\right)+N_1 \quad (22)$$

Similarly, the stress functions for the second hole are,

$$\phi_2(\zeta_2) = \frac{1}{s_1-s_2}\left\{\frac{1}{\zeta_2}\left(s_2\left(G_1+\overline{G_2}\right)-\left(G_3+\overline{G_4}\right)\right)+\frac{1}{{\zeta_2}^2}\left(s_2\left(G_2+\overline{G_1}\right)-\left(G_4+\overline{G_3}\right)\right)+N_2\right\}+B_1 z_{12} \quad (23)$$

$$\varphi_3(\zeta_3) = \frac{-1}{s_1-s_2}\left\{\frac{1}{\zeta_3}\left(s_1\left(G_1+\overline{G_2}\right)-\left(G_3+\overline{G_4}\right)\right)+\frac{1}{{\zeta_3}^2}\left(s_1\left(G_2+\overline{G_1}\right)-\left(G_4+\overline{G_3}\right)\right)+N_3\right\}+\left((B_2+iC_2)z_{23}\right) \quad (24)$$

2.3.5. Second Approximate Solution

In the second approximate solution, the first hole stress functions are transformed to the second hole center through transformation and rotation. This transformation introduces additional loading at the second hole, resulting in a new problem with negative boundary conditions. This problem is solved to obtain corrected stress functions. By superimposing the transformed and corrected stress functions, the final resultant stress functions for the holes are determined, thereby accounting for the interaction effects.

The first hole stress functions are transferred to the second hole center by translation by distance C_{12} in the mapped plane and rotation through the crack angle β_1. The C_{12} is obtained from

$$C_{12} = \frac{1}{2}\left[\frac{D_{12}}{M_1} + \sqrt{\left(\frac{{D_{12}}^2}{{M_1}^2}-4\right)}\right] \quad (25)$$

By transferring the stress function to the second hole center, we derive transformed stress functions at the second hole as $\phi_{12}{}^1(\zeta_2)$ and $\varphi_{12}{}^1(\zeta_2)$. The corrected stress functions are obtained by solving with negative boundary conditions, and the corrected stress functions for the second hole are represented as $\phi_{22}{}^1(\zeta_2)$ and $\varphi_{22}{}^1(\zeta_2)$.

The final stress functions for the second hole, which accounts for the interaction effect due to the first hole, are obtained by,

$$\phi_2{}^1(\zeta_2) = \phi_{12}{}^1(\zeta_2) + \phi_{22}{}^1(\zeta_2) \quad (26)$$

$$\varphi_2{}^1(\zeta_2) = \varphi_{12}{}^1(\zeta_2) + \varphi_{22}{}^1(\zeta_2) \quad (27)$$

Likewise, the stress functions$\phi_2{}^3(\zeta_2), \varphi_2{}^3(\zeta_2)$For the second hole, which accounts for interaction effects from the third hole, the results are obtained by the superposition of transformed stress functions. $\phi_{32}{}^3(\zeta_2)$, $\varphi_{32}{}^3(\zeta_2)$ and corrected stress functions $\phi_{22}{}^3(\zeta_2)$, $\varphi_{22}{}^3(\zeta_2)$.

$$\phi_2{}^3(\zeta_2) = \phi_{32}{}^3(\zeta_2) + \phi_{22}{}^3(\zeta_2) \quad (28)$$

$$\varphi_2{}^3(\zeta_2) = \varphi_{32}{}^3(\zeta_2) + \varphi_{22}{}^3(\zeta_2) \quad (29)$$

Final resultant stress functions $\phi_2(\zeta_2), \varphi_2(\zeta_2)$for the second hole, accounting for interaction effects of both the first and third holes, are obtained by superposition of Equation(26,27) and Equations (28,29)are as follows

$$\phi_2(\zeta_2) = \phi_2{}^1(\zeta_2) + \phi_2{}^3(\zeta_2) \quad (30)$$

$$\varphi_2(\zeta_2) = \varphi_2{}^1(\zeta_2) + \varphi_2{}^3(\zeta_2) \quad (31)$$

The derivatives of the stress function at second hole are

$$\phi_2{}^{1'}(\zeta_2) = \frac{1}{s_1-s_2}\left[H_{\phi_1}T_1^{'} + H_{\phi_2}T_1^{'} + H_{\phi_3}T_1^{'} + H_{\phi_4}T_1^{'} + H_{\phi_5}T_2^{'} + H_{\phi_6}T_2^{'} + H_{\phi_7}^{'} + H_{\phi_8}^{'} + N_1\right] + H_{\phi_9}^{'} + H_{\phi_{10}}^{'} \quad (32)$$

$$\varphi_2{}^{1'}(\zeta_2) = \frac{1}{s_2-s_1}\left[H_{\varphi_1}T_1^{'} + H_{\varphi_2}T_1^{'} + H_{\varphi_3}T_1^{'} + H_{\varphi_4}T_1^{'} + H_{\varphi_5}T_2^{'} + H_{\varphi_6}T_2^{'} + H_{\varphi_7}^{'} + H_{\varphi_8}^{'} + N_1\right] + H_{\varphi_9}^{'} + H_{\varphi_{10}}^{'} \quad (33)$$

Where,

$H_{\phi_1} = \left(\overline{s_1}-s_2\right)B_1M_1e^{2i(\beta_1)}$; $H_{\phi_2} = (\overline{s_1}-s_2)(\overline{a_3}+\overline{b_3})e^{2i(\beta_1)}$;

$H_{\phi_3} = \left(\overline{s_2}-s_2\right)(B_2-iC_2)M_1$; $H_{\phi_2} = (\overline{s_1}-s_2)(\overline{a_3}+\overline{b_3})e^{2i(\beta_1)}$; $H_{\phi_5} = -\left(\overline{s_2}-s_2\right)B_1M_1\overline{C_{12}}e^{2i(\beta_1)}$; $H_{\phi_6} = -(\overline{s_2}-s_2)(\overline{a_3}+\overline{b_3})\overline{C_{12}}e^{2i(\beta_1)}$;

$H_{\varphi_1} = \left(\overline{s_1}-s_1\right)B_1M_1e^{2i(\beta_1)}$; $H_{\varphi_2} = (\overline{s_1}-s_1)(\overline{a_3}+\overline{b_3})e^{2i(\beta_1)}$;

$H_{\varphi_3} = \left(\overline{s_2}-s_1\right)(B_2-iC_2)M_1$; $H_{\varphi_4} = (\overline{s_2}-s_1)(\overline{a_4}+\overline{b_4})M_1$;

$H_{\varphi 5} = -\left(\overline{s_2}-s_1\right)B_1M_1\overline{C_{12}}e^{2i(\beta_1)}$; $H_{\varphi 6} = -(\overline{s_2}-s_1)(\overline{a_3}+\overline{b_3})\overline{C_{12}}e^{2i(\beta_1)}$;

$H_{\phi 7}^{'} = -\left(\overline{s_1}-s_2\right)\frac{B_1M_1}{\zeta_2^2}$; $H_{\phi 8}^{'} = -(\overline{s_1}-s_2)\frac{(B_2-iC_2)M_1}{\zeta_2^2}e^{-2i(\beta_1)}$;

$$H_{\phi 9}^{'}=-\left[\frac{a_3+b_3}{\left(\zeta_2+C_{12}\right)^2 e^{2i(\beta_1)}}\right]; H_{\phi 10}^{'}=B_1\frac{M_1}{2}(a_1+b_1)\left[1-\frac{e^{-2i(\beta_1)}}{(\zeta_2+C_{12})^2}\right];$$

$$H_{\varphi 7}^{'}=-\left(\overline{s_1}-s_1\right)\frac{B_1M_1}{\zeta_2^2}; H_{\varphi 8}^{'}=-(\overline{s_1}-s_1)\frac{(B_2-iC_2)M_1}{\zeta_2^2}e^{-2i(\beta_1)};$$

$$H_{\phi_1}=\left(\overline{s_1}-s_2\right)B_1M_1e^{2i(\beta_1)}; H_{\phi_2}=(\overline{s_1}-s_2)(\overline{a_3}+\overline{b_3})e^{2i(\beta_1)};$$

$$H_{\phi_3}=\left(\overline{s_2}-s_2\right)(B_2-iC_2)M_1; H_{\phi_2}=(\overline{s_1}-s_2)(\overline{a_3}+\overline{b_3})e^{2i(\beta_1)};$$

$$H_{\phi_5}=-\left(\overline{s_2}-s_2\right)B_1M_1\overline{C_{12}}e^{2i(\beta_1)}; H_{\phi_6}=-(\overline{s_2}-s_2)(\overline{a_3}+\overline{b_3})\overline{C_{12}}e^{2i(\beta_1)};$$

$$H_{\varphi_1}=\left(\overline{s_1}-s_1\right)B_1M_1e^{2i(\beta_1)}; H_{\varphi_2}=(\overline{s_1}-s_1)(\overline{a_3}+\overline{b_3})e^{2i(\beta_1)};$$

$$H_{\varphi_3}=\left(\overline{s_2}-s_1\right)(B_2-iC_2)M_1; H_{\varphi_4}=(\overline{s_2}-s_1)(\overline{a_4}+\overline{b_4})M_1;$$

$$H_{\varphi 5}=-\left(\overline{s_2}-s_1\right)B_1M_1\overline{C_{12}}e^{2i(\beta_1)}; H_{\varphi 6}=-(\overline{s_2}-s_1)(\overline{a_3}+\overline{b_3})\overline{C_{12}}e^{2i(\beta_1)};$$

$$H_{\phi 7}^{'}=-\left(\overline{s_1}-s_2\right)\frac{B_1M_1}{\zeta_2^2}; H_{\phi 8}^{'}=-(\overline{s_1}-s_2)\frac{(B_2-iC_2)M_1}{\zeta_2^2}e^{-2i(\beta_1)};$$

$$H_{\phi 9}^{'}=-\left[\frac{a_3+b_3}{\left(\zeta_2+C_{12}\right)^2 e^{2i(\beta_1)}}\right]; H_{\phi 10}^{'}=B_1\frac{M_1}{2}(a_1+b_1)\left[1-\frac{e^{-2i(\beta_1)}}{(\zeta_2+C_{12})^2}\right];$$

$$H_{\varphi 9}^{'}=\left[\left[\frac{a_4+b_4}{(\zeta_2+C_{12})^2}\right]+(B_2+iC_2)\frac{M_1}{2}(a_1+b_1)\left(e^{2i(\beta_1)}-\frac{1}{(\zeta_2+C_{12})^2}\right)\right];$$

$$H_{\varphi 10}^{'}=\left[2\overline{C_{12}}\left\{\left[\frac{a_3+b_3}{\left(\zeta_2+C_{12}\right)^2 e^{2i(\beta_1)}}\right]+\frac{M_1}{2}\left(a_1+b_1\right)\left(\frac{e^{-2i(\beta_1)}}{\left(\zeta_2+C_{12}\right)^3}\right)\right\}\right]$$

$$T_1^{'}=\frac{1}{(1+\zeta_2\overline{C_{12}})^2}, T_2^{'}=\frac{2\zeta_2}{(1+\zeta_2\overline{C_{12}})^3}$$

Similarly, the derivatives of the stress functions associated with the second hole, considering the interaction effect from the third hole, are obtained by considering the respective center distance.

By applying superposition, the derivatives of the final stress functions $\phi_2{}'(\zeta_2)$, and$\varphi_2{}^1(\zeta_2)$At the second hole, the results are obtained. Following a similar process, the derivatives of the final stress functions $\phi_1{}'(\zeta_1), \varphi_1{}^1(\zeta_1)$ at the first hole, as well as derivatives of the final stress functions $\phi_3{}'(\zeta_3), \varphi_3{}^1(\zeta_3)$At the third hole, the following are also derived.

2.4. Stress Intensity Factors (SIFs)

The SIFs for mode-I(K_I) and mode-II (K_{II}) at crack tips of the second hole are obtained by the following relation given by Cheong and Hong [14].

$$K_I+\frac{K_{II}}{s_2}=2\sqrt{\frac{\pi}{L}}\left(\frac{s_2-s_1}{s_2}\right)\phi_2{}'(\zeta_2) \quad (34)$$

$$K_I+\frac{K_{II}}{s_1}=2\sqrt{\frac{\pi}{L}}\left(\frac{s_1-s_2}{s_1}\right)\varphi_2{}'(\zeta_2) \quad (35)$$

3. Results and Discussions

The general solution for determining the SIF in an infinite orthotropic plate featuring three holes and two cracks extending from each hole is derived using CVM and the Schwarz alternating method. The analytical results of the fundamental formulation are computed with MATLAB R2020a.

Assumptions adopted in the derivation:

1. The plate material is assumed to be homogeneous, orthotropic, and to exhibit linear elastic behavior.
2. The Plate is considered sufficiently large in comparison with the hole and crack dimensions, so boundary effects are neglected.
3. A two-dimensional stress state is assumed, and thickness effects are ignored.
4. The applied loading is uniform and acts at infinity.
5. Residual stresses, plastic deformation, and material nonlinearity are not considered.

3.1. Stepwise Procedure for Analytical Results

1. Select the geometric parameters such as crack lengths a, b, c, d, e, f, radius of holes, and crack orientation angle β_1, among others.
2. Choose the material and document its properties along with the fiber direction.
3. Determine the compliance coefficients a_{ij}.
4. The Roots of the bi-harmonic equation are computed using MATLAB code.
5. Constants B_1, B_2, C_2, a_1, a_2, b_1, b_2, a_3, b_3, a_4, b_4, G_1, G_2, G_3, and G_4 are calculated.
6. The derivatives of the final resultant stress functions for all holes are derived.
7. Calculated the normalized SIF by using the relation $K_0=P\sqrt{\pi L}$.
8. The normalized SIF ratios (K_I/K_0, K_{II}/K_0) are computed, and their variations are plotted against different geometric parameters.

3.2. Effect of Various Parameters on 3 Holes-Crack System Subjected to Biaxial+Shear Loading

The results obtained with E-Glass/Epoxy material at a fiber orientation of 0^0, P=1, and a loading factor of λ=1 apply in all instances.

3.2.1. Effect of Center Distance between Holes on SIF Ratios

For analyzing the Effect of center distance between holes, the parameters considered are as follows: radii of holes $R_1=R_2=R_3=2$ mm, crack lengths a=b=c=d=e=f=2 mm, crack angle $\beta_1=0$, and the center distance $D=D_{12}=D_{23}$ varied from 10 mm to 50 mm with an interval of 5 mm and hole size constant$L = \frac{2R_2+a+b}{2}$.

Table 1. Effect of centre distance between holes on SIFs ratios at second hole crack tips

L/D	crack tip-c		crack tip-d	
	KI/K0	KII/K0	KI/K0	KII/K0
0.400	3.0579	1.6639	3.0578	1.6639
0.267	2.3704	1.1995	2.3715	1.2006
0.200	2.2369	1.1376	2.2371	1.1356
0.160	2.2091	1.1258	2.2098	1.1263
0.133	2.1914	1.1166	2.1904	1.1156
0.114	2.1799	1.0822	2.1881	1.0829
0.100	2.1855	1.0495	2.1859	1.0506
0.089	2.1836	1.0241	2.1839	1.0246
0.080	2.1823	1.0130	2.1824	1.0139

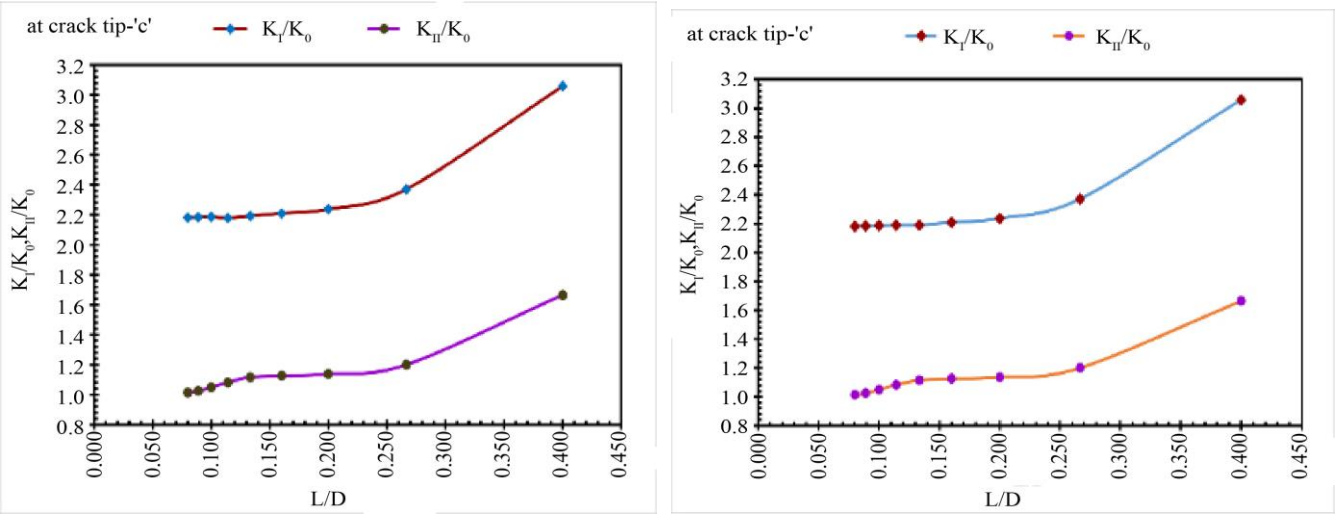

(a) **(b)**

Fig. 4 (a) & (b) Effect of center distance between holes on SIF ratio

As the distance between the centers of the holes increases, the interaction between them weakens. This reduction in interaction leads to lower maximum stress at the crack tips and a gradual decrease in the normalized Stress Intensity Factor (SIF) ratios. When the holes are closer together, the normalized SIF ratio is noticeably higher, indicating strong interaction effects. However, as the center distance increases, the normalized SIF ratio continues to decrease, with the K_{II}/K_0 value approaching 1, which suggests that the interaction between the holes becomes negligible. Beyond an L/D value of about 0.2, the normalized SIF ratios stabilize, a trend that is clearly shown in Figure 4. This behavior is consistently observed at both crack tip-c and crack tip-d for the Mode-I and Mode-II normalized SIF ratio.

3.2.2. Effect of Crack Lengths on SIF Ratios

For analyzing the Effect of varying crack lengths, the parameters considered are as follows: radii of holes $R_1=R_2=R_3=R=2$ mm, crack lengths a=b=e=f=2 mm, crack angles $\beta_1=0$, the center distance $D_{12}=20$ mm, and $D_{23}=20$ mm, and the crack lengths (c, d) are varied from 2 mm to 6 mm with an interval of 0.5 mm.

Table 2. Effect of varying crack lengths on SIF ratios at second hole crack tips

c/R	crack tip-c		crack tip-d	
	K_I/K_0	K_{II}/K_0	K_I/K_0	K_{II}/K_0
1	2.2914	1.1348	2.2909	1.1341
1.25	2.3874	1.2837	2.3869	1.2832
1.5	2.4834	1.4026	2.4828	1.4019
1.75	2.5456	1.4566	2.5452	1.4559
2	2.5854	1.4805	2.5849	1.4798
2.25	2.6021	1.5251	2.6014	1.5248
2.5	2.6234	1.5697	2.623	1.5692
2.75	2.6554	1.5941	2.6548	1.5934
3	2.7239	1.6184	2.7232	1.6181

As the dimensionless parameter c/R increased gradually, the interaction effect between the holes intensified, leading to higher maximum stress values at the crack tips and, ultimately, an increase in both SIFs ratio values at the crack. The Mode-I SIF ratio is consistently higher than the Mode-II SIF ratio across the entire range of c/R. From Figure 5**,** as the dimensionless ratio c/R increases, the SIF ratios also rise gradually, but Mode-I is more significant than Mode-II.

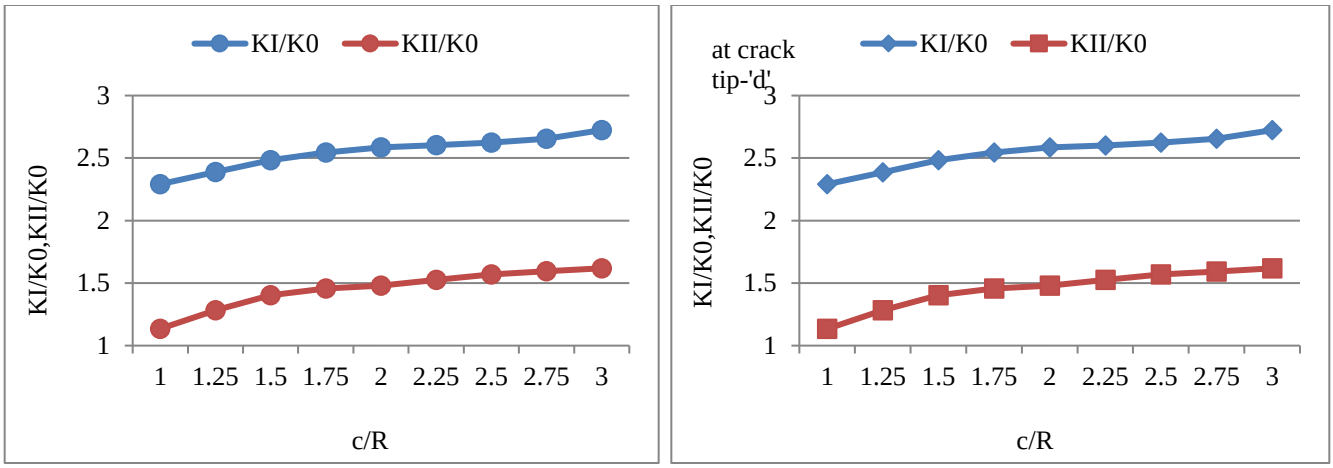

(a) **(b)**

Fig. 5 (a) & (b) Effect of varying crack length on SIF ratio

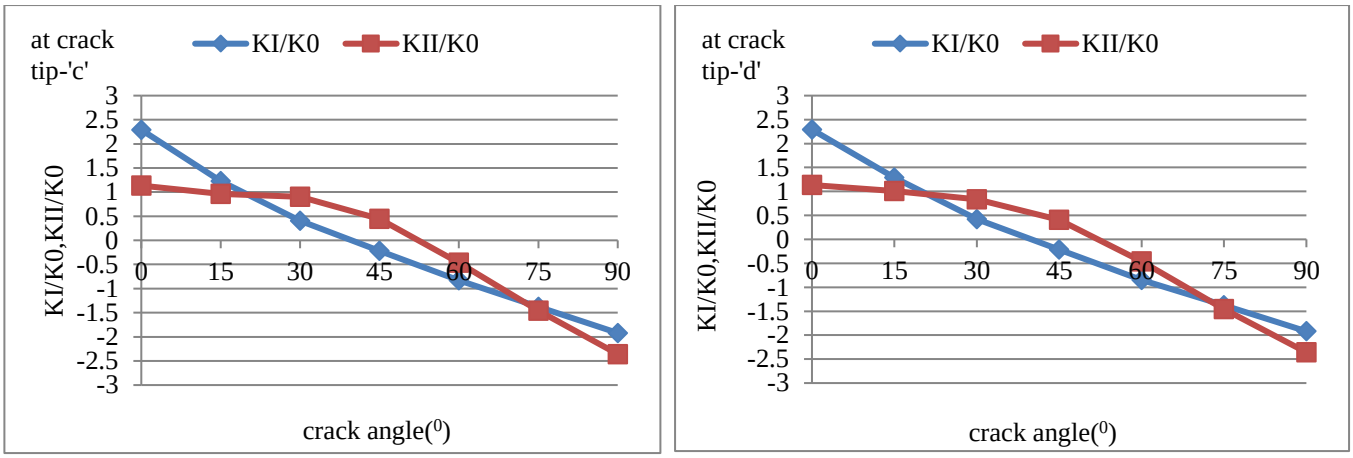

(a) **(b)**

Fig. 6 (a) & (b) Effect of varying crack angle on SIF ratio

3.2.3. Effect of Crack Angle on SIF Ratios

For analyzing the Effect of crack angle, the parameters considered are as follows: radii of holes $R_1=R_2=R_3=2$ mm, crack lengths a=b=c=d=e=f=2 mm, crack angle at the second hole 'β_1' varied from 0^0 to 90^0, the center distance $D_{12}=20$ mm, and $D_{23}=20$ mm.

Table 3. Effect of varying crack angle on SIF ratios at second hole crack tips

β_1	crack tip-c		crack tip-d	
	K_I/K_0	K_{II}/K_0	K_I/K_0	K_{II}/K_0
0^0	2.2914	1.1348	2.2909	1.1341
15^0	1.226	0.9608	1.2857	1.0082
30^0	0.4081	0.9006	0.4196	0.837
45^0	-0.2193	0.4443	-0.2131	0.4096
60^0	-0.8266	-0.4669	-0.8508	-0.4606
75^0	-1.3768	-1.461	-1.3761	-1.4588
90^0	-1.9209	-2.3581	-1.92	-2.3581

As illustrated in Figure 6**,** variation in the crack angle at the second hole changes, mode-I SIF ratio(K_I/K_0)attains a positive maximum at 0^0 , then decreases gradually, crosses zero at approximately 60^0, becomes negative beyond this angle, and reaches a negative maximum at 90^0.

Similarly, the mode-II SIF ratio (K_{II}/K_0) also shows a positive maximum at 0^0, decreases steadily up to about 50^0, after which it drops sharply, crosses zero near 55^0, and becomes negative, attaining its negative peak at 90^0.

The mode-I and mode-II SIF ratio curves intersect at a crack angle close to 20^0, indicating an equal influence from both modes at this crack angle. At lower crack angles, the mode-I behaviour is dominant; as the crack angle increases, mode-II behavior becomes more significant relative to mode-I.

Overall, the variation of SIF ratios at both crack tips varies with variation in the crack angle, indicating the strong sensitivity of fracture behavior to crack orientation.

3.2.4. Effect of Fiber Angle on SIF Ratios

For analyzing the Effect of fiber angle, the parameters considered are as follows: radii of holes $R_1=R_2=R_3=2$ mm, crack lengths a=b=c=d=e=f=2 mm, crack angle at second hole $\beta_1=0^0$, and fiber angle (θ) varied from 0^0 to 90^0, and the center distances $D_{12}=20$ mm and $D_{23}=20$ mm.

Table 4. Effect of varying fiber angle on SIF ratios at second hole crack tips

θ	crack tip-c		crack tip-d	
	K_I/K_0	K_{II}/K_0	K_I/K_0	K_{II}/K_0
0^0	2.2914	1.1348	2.2909	1.1341
10^0	1.5726	-3.8678	1.6838	-3.9675
20^0	64.222	49.9228	63.9431	50.4089
30^0	2.7064	-1.149	2.6703	-1.3239
40^0	0.9135	-1.3925	0.808	-1.574
50^0	29.7545	9.6497	30.4875	9.4186
60^0	-11.5798	3.9375	-11.714	4.2859
70^0	-2.0541	4.6317	-2.0019	4.8123
80^0	1.8637	3.1439	1.9703	3.2319
90^0	2.2905	1.1348	2.2915	1.1341

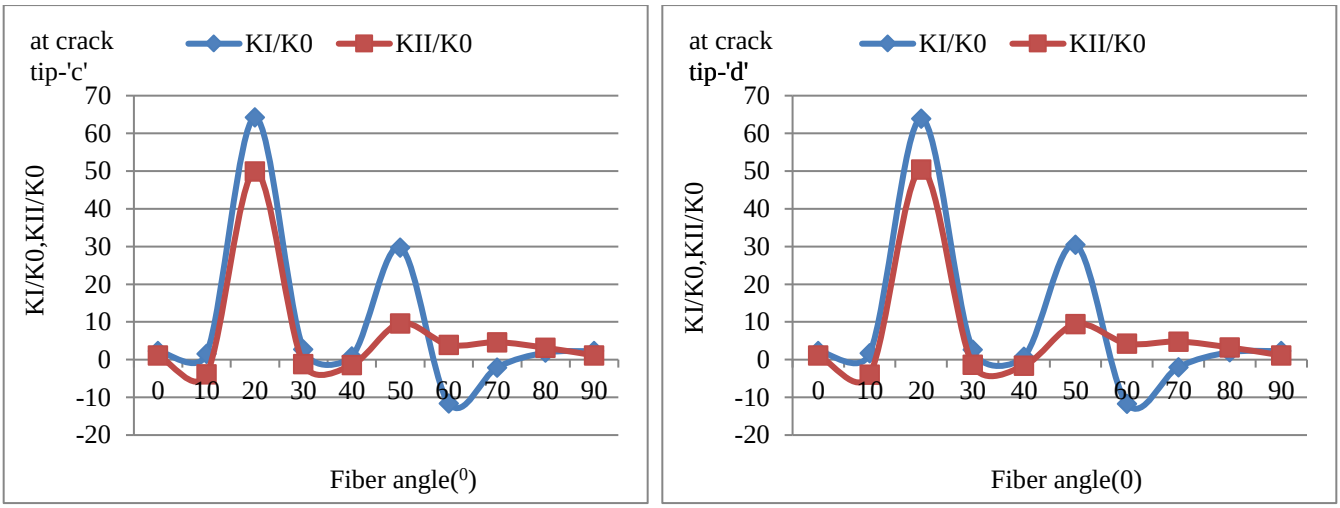

(a) **(b)**

Fig. 7 (a) & (b) Effect of varying fiber angle on SIF ratio

As shown in Figure 7**,** varying fiber angle from 0^0 to 90^0, has a clear influence on both mode-I (K_I/K_0) and mode-II (K_{II}/K_0) SIF ratios. Both modes exhibit a peak at approximately 20^0, along with a secondary peak near 50^0. The SIF ratios drop to zero at several intermediate fiber angles, notably around 10^0,30^0, and 40^0, while nearly identical SIF ratios are observed for both modes at 0^0 and 90^0. The mode-I SIF ratio values are predominantly positive, with the exception of negative values that appear, namely near 10^0, between 30^0 and 40^0, and between 55^0 and 70^0. In contrast, the mode-II SIF ratio K_{II}/K_0 remains largely positive, with negative values occurring only near 10^0 and between $30^0$and 40^0. Overall, the variation of SIF ratios at the crack tips with changing fiber angle demonstrates that the fiber angle has a significant impact on the SIF ratios.

3.2.5. Effect of Material on SIF Ratios

For analyzing the Effect of material, the parameters considered are as follows: radii of holes $R_1=R_2=R_3=2$ mm, crack lengths a=b=c=d=e=f=2 mm, crack angle at second hole $\beta=0^0$, and fiber angle (θ)=0^0, and the center distances $D_{12}=10$ mm and $D_{23}=10$ mm.

Table 5. Effect of material on SIFs ratios at second hole crack tips

Material	crack tip-c		crack tip-d	
	K_I/K_0	K_{II}/K_0	K_I/K_0	K_{II}/K_0
Graphite/Epoxy	3.0565	1.6631	3.0578	1.6639
Boron/Epoxy	3.0146	1.2521	3.0154	1.2528
E-Glass/Epoxy	2.9602	1.5846	2.9608	1.5854
Carbon/Epoxy	3.2326	1.2091	3.2333	1.2097
S-Glass/Epoxy	2.9084	1.2309	2.9092	1.2317

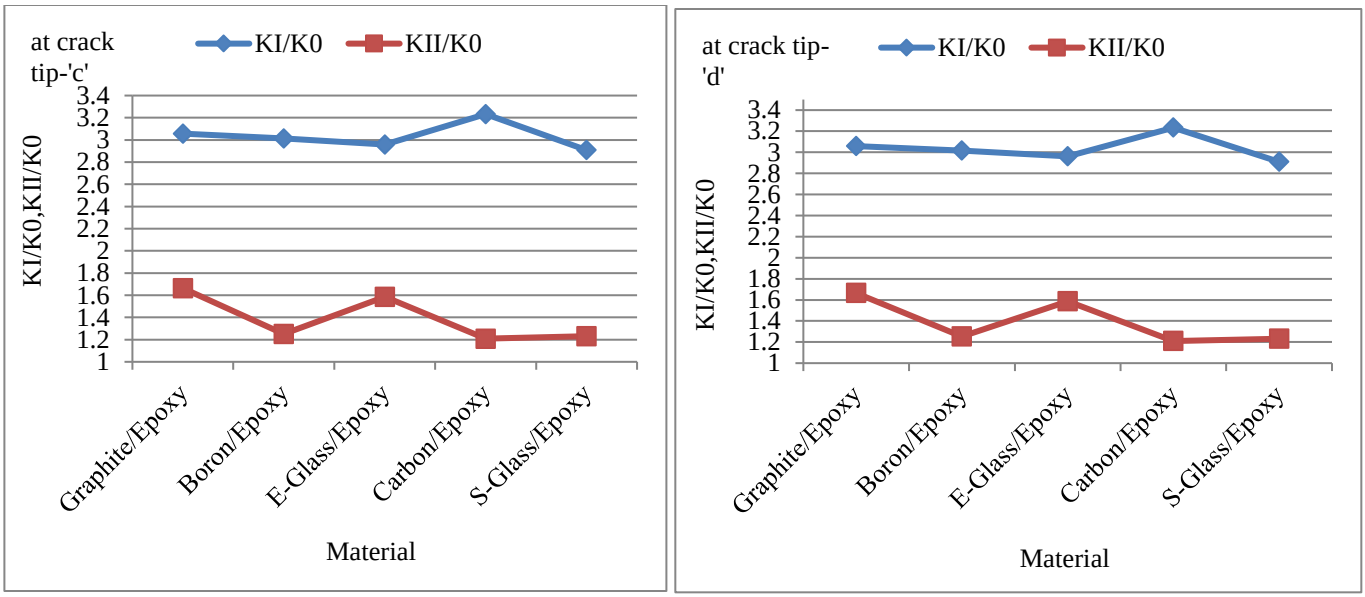

Fig. 8 (a) & (b) Effect of material on SIF ratio

From Figure 8, it is evident that the mode-I SIF ratio(K_I/K_0) is significantly higher than the mode-II ratio K_{II}/K_0, being approximately twice its magnitude. The K_I/K_0 values vary from 2.9084 (for S-Glass/Epoxy) to 3.2326 (for Carbon/Epoxy). In contrast, the K_{II}/K_0 values show comparatively smaller variation, ranging from 1.2091 (for Carbon/Epoxy) to 1.6631 (for Graphite/Epoxy). Notably, no single material exhibits the maximum SIF ratio for both mode-I and mode-II simultaneously. The results demonstrate a significant influence of the material properties on the SIF ratios.

3.3. Numerical Results with ANSYS

An orthotropic plate with three holes and two radial cracks emanating from each hole is modelled in ANSYS. The procedure involves assigning material properties, creating a coordinate system at crack tips, defining nodal sections at these crack tips, meshing the geometry, and configuring boundary conditions and loads. ANSYS static analysis is then performed to obtain crack tip stresses and nearby directional displacement values.

The deformation values collected from the nodes near the crack tip are utilized to determine the SIF values through the Displacement Correlation Method (DCT) as described by Kim et al. [13]. The problem is modeled in ANSYS using approximately 64,000 elements, with a sphere of influence–based mesh refinement applied near the crack tips. The resulting RMSE values remain below 3%.

3.3.1. Comparison of the Effect of Crack Angle on SIFs Ratio

For analyzing the Effect of crack angle, the parameters considered are as follows: radii of holes $R_1=R_2=R_3=2$ mm, crack lengths a=b=c=d=e=f=2 mm, crack angle at the second hole β_1 varied from 0^0 to 90^0, the center distance $D_{12}=20$ mm, and $D_{23}=20$ mm.

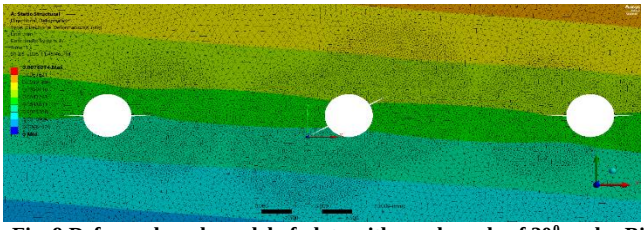

Fig. 9 Deformed mesh model of plate with crack angle of 30^0 under Bi-Axial+Shear loading

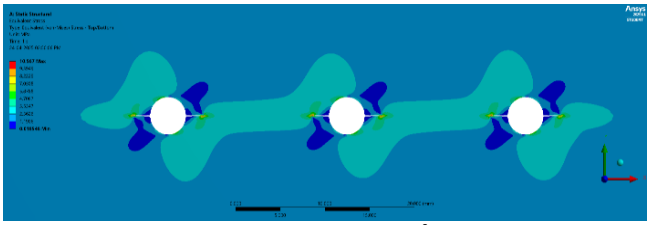

Fig. 10 Stress distribution with 0^0 crack angle

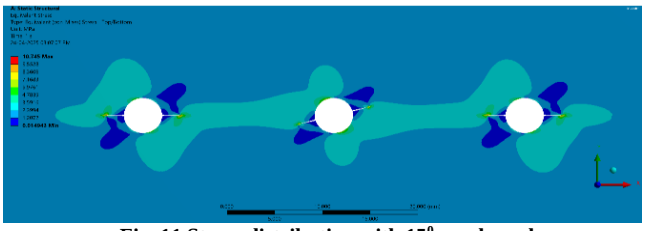

Fig. 11 Stress distribution with 15^0 crack angle

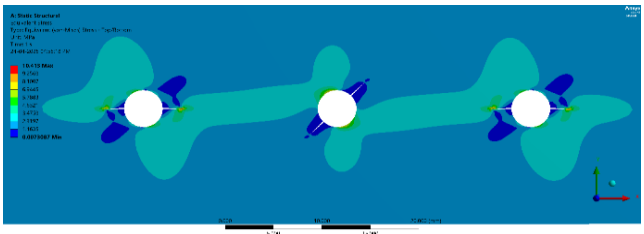

Fig. 12 Stress distribution with 45^0 crack angle

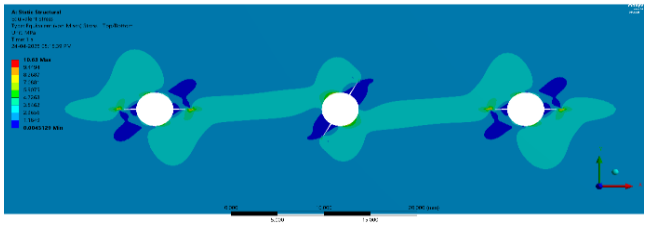

Fig. 13 Stress distribution with 60^0 crack angle

Figure 9 illustrates the meshing surrounding the cracks along with the deformation pattern. The Numerical results obtained from ANSYS for the E-Glass/Epoxy plate, as shown in Figures (10, 11, 12, & 13), reveal that the interaction effect is greater when the angle of the crack is at 45^0 and a strong shear alignment among the neighboring holes.

Table 6. Comparison of analytical and numerical results with varying crack angle

β_1	at crack tip-c			at crack tip-c		
	Analytical Solution-K_I/K_0	**ANSYS Solution-K_I/K_0**	**Difference (%)**	**Analytical Solution-K_{II}/K_0**	**ANSYS Solution-K_{II}/K_0**	**Difference (%)**
0^0	2.2914	2.1823	4.76	1.1348	1.0699	5.72
15^0	1.226	1.1885	3.06	0.9608	0.9257	3.65
30^0	0.4081	0.4214	-3.25	0.9006	0.8580	4.73
45^0	-0.2193	-0.2078	5.24	0.4443	0.4589	-3.29
60^0	-0.8266	-0.8614	-4.21	-0.4669	-0.4873	-4.36
75^0	-1.3768	-1.3373	2.87	-1.461	-1.3903	4.84
90^0	-1.9209	-1.8571	3.32	-2.3581	-2.2668	3.87

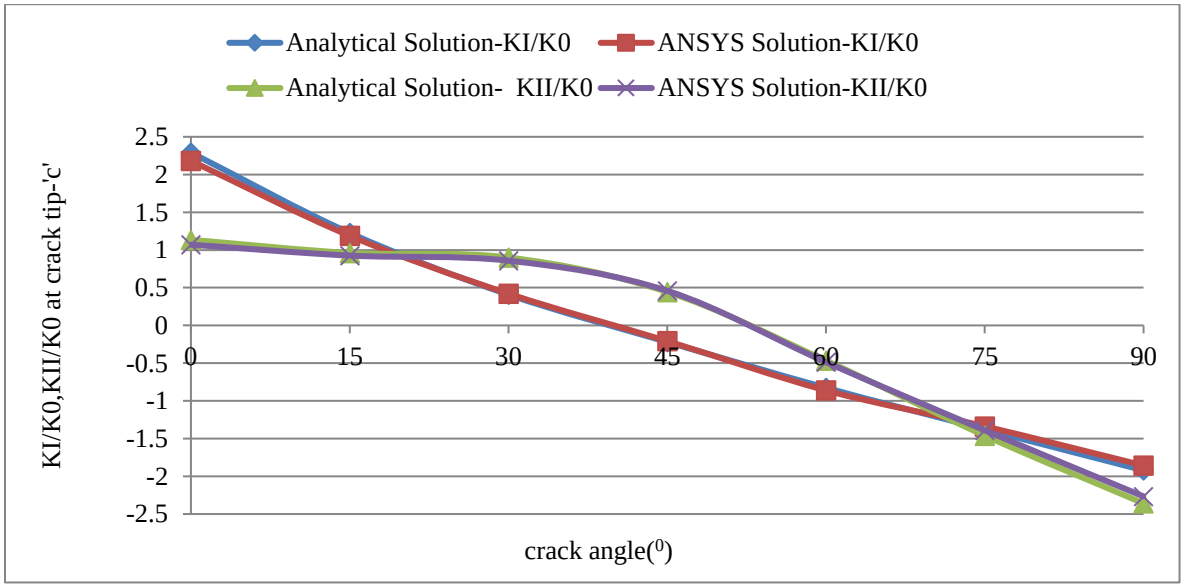

Fig. 14 Comparison of analytical results with numerical results for crack angle varying case

From Figure 14, it is observed that analytical results and numerical results obtained from ANSYS show close agreement for both K_I/K_0 and K_{II}/K_0over the entire range of crack angles. The difference between analytical and numerical results remains within 6%, thereby confirming that ANSYS results strongly support the analytical findings.

4. Conclusion

The analytical solution is developed for an orthotropic plate containing three circular holes, each containing two cracks, obtained by the complex variable method. The interaction effect between neighboring cracked holes is analyzed through the Schwartz alternating technique. To the author's knowledge, the problem of three cracked holes with interaction effects has not been previously reported in the literature.

The results show that, under combined loading, as crack length increases, it leads to a higher SIF ratio, whereas an increased center distance results in a lower SIF ratio, which

stabilizes beyond a certain distance. The crack angle and fiber angle significantly influence the SIF ratios.

Additionally, the SIF ratio at the inner crack tips is greater than that at the outer crack tips. The analytical method results are validated against ANSYS simulation solutions for selected cases, showing a difference of less than 6%, demonstrating good agreement. The proposed analytical solution is limited to orthotropic plates and is not directly applicable to fully anisotropic plates.

In addition, the adopted mapping function is restricted to cracks emanating from circular holes and cannot be extended to cracks originating from holes of varying shapes. Nevertheless, the methodology can be extended to multilayered composite plates. The current method's simple steps make it easier to apply in real-world fracture analysis of composite structures like rockets and airplanes.

Within the constraints of linear elastic behavior and two-dimensional assumptions, the suggested formulation can be applied to orthotropic plates with multiple holes and cracks under combined in-plane loading. The method's application is limited by idealized geometry, loading applied at infinity, and the disregard for finite boundary effects, material nonlinearity, and crack growth, even though it systematically and analytically captures interaction effects.

Future research could use a combination of analytical and numerical methods to address nonlinear material response, crack growth, and expand the current model to finite plates.

Nomenclature

a_{ij}	Elastic constants	[ ]
P	Stress	[MPa]
a_1, a_2, b_1, b_2	complex variables	[ ]
R_1, R_2, R_3	Radius of holes	[mm]
a,b,c,d,e,f	Lengths of cracks	[mm]
Re	Real part	[ ]
a_3,a_4,b_3,b_4	Simplification terms	[ ]
s_i	Complex parameter	[ ]
B_1,B_2,C_2	Loading constants	[ ]
SIF	Stress Intensity Factor	[Mpa-$\sqrt{mm}$]
C_{12}, C_{23}	Distance in ζ-plane	[ ]
D_{12}, D_{23}	Distance in z-plane	[ ]
z_i	Complex number	[ ]
f_1, f_2	Boundary conditions	[ ]
β_1,β_2	Crack angles	[ ]
I	Imaginary unit	[ ]
ζ	Complex number in mapped plane	
Im	Imaginary part	[ ]
$w_j(\zeta)$	Mapping function	[ ]
K_0	Normalized SIF	[Mpa-$\sqrt{mm}$]
$\phi_1(z_1)$, $\varphi_1(z_2)$	Stress functions	[ ]
K_I, K_{II}	Mode-I, Mode-II SIF	[Mpa-$\sqrt{mm}$]

Acknowledgments

The authors are grateful to the Department of Mechanical Engineering, JNTUA, for providing the resources and assistance required to carry out this work. This research received no external financial funding.

References

[1] Seyyed Hassan Moussavian, Mohammad Jafari, and Mojtaba Hajimohammadi, "Analytical Calculation of Stress Intensity Factors for Orthotropic Plates Containing Cracks Emanating from a Circular Hole using Schwarz Integration," *ZAMM - Journal of Applied Mathematics and Mechanics*, vol. 104, no. 2, pp. 1-16, 2023. [CrossRef] [Google Scholar] [Publisher Link]

[2] Rahmatollah Ghajar, and Mojtaba Hajimohamadi, "Analytical Calculation of Stress Intensity Factors for Cracks Emanating from a Quasi-square Hole in an Infinite Plane," *Theoretical and Applied Fracture Mechanics*, vol. 99, pp. 71-78, 2019. [CrossRef] [Google Scholar] [Publisher Link]

[3] Giuseppe Catalanotti, Rui M. Salgado, and Pedro P. Camanho, "On the Stress Intensity Factor of Cracks Emanating from Circular and Elliptical Holes in Orthotropic Plates," *Engineering Fracture Mechanics*, vol. 25, 2021. [CrossRef] [Google Scholar] [Publisher Link]

[4] H.G. Beom, and C.B. Cui, "Oblique Edge Crack in an Anisotropic Material under Antiplane Shear," *European Journal of Mechanics - A/Solids*, vol. 30, no. 6, pp. 893-901, 2011. [CrossRef] [Google Scholar] [Publisher Link]

[5] H. Goleij, R.T. Faal, and A.R. Fotuhi, "Mixed Mode Cracks in Annular Planes of Cylindrical Orthotropy Subjected to Inplane Loading," *Theoretical and Applied Fracture Mechanics*, vol. 93, pp. 1-18, 2018. [CrossRef] [Google Scholar] [Publisher Link]

[6] Volodymyr I. Kushch, and Igor Sevostianov, "Ellipsoidal Inhomogeneity in Elliptically Orthotropic Elastic Solid," *International Journal of Solids and Structures*, vol. 206, pp. 282-291, pp. 1-10, 2020. [CrossRef] [Google Scholar] [Publisher Link]

[7] Jianwei Huang et al., "Analysis of Stress Intensity Factor for a Crack Emanating from Elliptical Hole Subjected to Compressive Stress and Shear Stress," *Theoretical and Applied Fracture Mechanics*, vol. 120, 2022. [CrossRef] [Google Scholar] [Publisher Link]

[8] V.G. Ukadgaonker, and D.S. Sharma, "Stress Intensity Factors for Internally Loaded Crack in a Composite Plate Subjected to Arbitrary Biaxial Loading at Infinity," *International Journal of Design Engineering*, vol. 2, no. 2, pp. 136-153, 2009. [Google Scholar] [Publisher Link]

[9] Jinfang Zhao et al., "A Method for Stress Intensity Factor Calculation of Infinite plate Containing Multiple Hole-Edge Cracks," *International Journal of Fatigue*, vol. 35, no. 1, pp. 2-9, 2012. [CrossRef] [Google Scholar] [Publisher Link]

[10] Xiangqiao Yan, "An Empirical Formula for Stress Intensity Factors of Cracks Emanating from a Circular Hole in a Rectangular Plate in Tension," *Engineering Failure Analysis*, vol. 14, no. 5, pp. 935-940, 2007. [CrossRef] [Google Scholar] [Publisher Link]

[11] Shuhong Liu, and Shijie Duan, "Analytical Solutions of Cracks Emanating from an Elliptic Hole in an Infinite Plate Under Tension," *Chinese Journal of Mechanical Engineering*, vol. 27, pp. 1057-1063, 2014. [CrossRef] [Google Scholar] [Publisher Link]

[12] R. Harilal, C.P. Vyasarayani, and M. Ramji, "A Linear Least Squares Approach for Evaluation of Crack Tip Stress Field Parameters using DIC," *Optics and Lasers in Engineering*, vol. 75, pp. 95-102, 2015. [CrossRef] [Google Scholar] [Publisher Link]

[13] Jeong-Ho Kim, and Glaucio H. Paulino, "Mixed-Mode Fracture of Orthotropic Functionally Graded Materials using Finite Elements and the Modified Crack Closure Method," *Engineering Fracture Mechanics*, vol. 69, pp. 1557-1586, no. 14-16, 2002. [CrossRef] [Google Scholar] [Publisher Link]

[14] S.K. Cheong, and C.S. Hong, "Analysis of Cracks Emanating from a Circular Hole in an Orthotropic Plate under Mixed Mode Deformation," *Engineering Fracture Mechanics*, vol. 31, no. 2, pp. 237-248, 1988. [CrossRef] [Google Scholar] [Publisher Link]

[15] Dong-shan Fu, and Xing Zhang, "Analytical-variational Method of Solution for Stress Intensity Factors about Anisotropic and Isotropic Finite Plates with Double Cracks Emanating from Holes," *Engineering Fracture Mechanics*, vol. 50, no. 3, pp. 311-324 1995. [CrossRef] [Google Scholar] [Publisher Link]

[16] Xin-Lin Gao, "A General Solution of an Infinite Elastic Plate with an Elliptic Hole under Biaxial Loading," *International Journal of Pressure Vessels and Piping*, vol. 67, no. 1, pp. 95-104, 1996. [CrossRef] [Google Scholar] [Publisher Link]

[17] IIvan Stephen Sokolnikoff, *Mathematical Theory of Elasticity*, McGraw-Hill, pp. 1-476, 1956. [Google Scholar] [Publisher Link]

[18] Sergeĭ Georgievich Lekhnit͡skiĭ, *Anisotropic Plates*, Gordon and Breach, pp. 1-534, 1968. [Google Scholar] [Publisher Link]

[19] Nikolaĭ Ivanovich Muskhelishvili, *Some Basic Problems of the Mathematical Theory of Elasticity: Fundamental Equations, Plane Theory of Elasticity, Torsion, and Bending*, pp. 1-718, 1963. [Google Scholar] [Publisher Link]

[20] Ashish Patel, and Chaitanya K. Desai, "Stress Concentration around an Elliptical Hole in a Large Rectangular Plate Subjected to Linearly Varying In-Plane Loading on Two Opposite Edges," *Theoretical and Applied Fracture Mechanics*, vol. 106, 2020. [CrossRef] [Google Scholar] [Publisher Link]

[21] George C. Sih, *Methods of Analysis and Solution of Crack Problems Recent Developments in Fracture Mechanics, Theory and Methods of Solving Crack Problems*, Noordhoff International Publishing, pp. 1-517, 1973. [Google Scholar] [Publisher Link]

[22] V.G. Ukadgaonker, and A.P. Naik, "Interaction Effect of Two Arbitrarily Oriented Cracks — Part I," *International Journal of Fracture*, vol. 51, pp. 219-230, 1991. [CrossRef] [Google Scholar] [Publisher Link]

[23] V.G. Ukadgaonker, and D.K.N. Rao, "A General Solution for Stresses around Holes in Symmetric Laminates under Inplane Loading," *Composite Structures*, vol. 49, no. 3, pp. 339-354, 2000. [CrossRef] [Google Scholar] [Publisher Link]

[24] O.L. Bowie, "Analysis of an Infinite Plate Containing Radial Cracks Originating at the Boundary of an Internal Circular Hole," *Journal of Mathematics and Physics*, vol. 35, no. 1-4, pp. 60-71, 1956. [CrossRef] [Google Scholar] [Publisher Link]

[25] M. Chafi, and A. Boulenouar, "A Numerical Modelling of Mixed Mode Crack Initiation and Growth in Functionally Graded Materials," *Materials Research*, vol. 22, no. 3, pp. 1-10, 2019. [CrossRef] [Google Scholar] [Publisher Link]